

Rheological, thermal and tensile properties of PE/nanoclay nanocomposites and PE/nanoclay nanocomposite cast films

Mehdi Haji Abdolrasouli^{1*}, Amir Babaei²

¹Department of Industrial Engineering, Faculty of Engineering, University of Hormozgan, Bandar-Abbas, Iran

²Department of Polymer Engineering, Faculty of Engineering, Golestan University, Gorgan, Iran

Received: 11 July 2017, Accepted: 3 September 2017

ABSTRACT

The effects of three different mixers, two different feeding orders and nanoclay content on the structure development and rheological properties of PE/nanoclay nanocomposite samples were investigated. Fractional Zener and Carreau–Yasuda models were applied to discuss the melt linear viscoelastic properties of the samples. Moreover, scaling law for fractal networks was used to quantify the clay dispersion, which depends on the PE matrix structure. A better dispersion and a higher melt intercalation of nanoclay particles were obtained by simultaneous feeding compared to compatibilizer/nanoclay masterbatch feeding. A twin-screw extruder (Brabender DSE 25 model) showed a greater potential for melt intercalation of PE/nanoclay as compared to internal mixers (Brabender W50 and Haake Rheomix 3000 batch mixers). Comparing the thermal analysis of PE, PE/PE-g-MA and PE/nanoclay samples by DSC technique showed an opposite effect for the compatibilizer versus the nanoclay on the crystallization behavior of PE. PE/nanoclay cast film samples were produced at three different draw ratios. The X-ray diffraction structural analysis in conjunction with the melt linear viscoelastic measurements confirmed that the PE/nanoclay cast film produced at higher draw ratio had a more effective melt intercalation. The tensile test showed that the machine direction modulus and yield strength of both PE and PE/nanoclay cast film samples reduced with increase of the draw ratio. **Polyolefins J (2018) 5:47-58**

Keywords: Polyethylene; nanocomposite; film; rheology; tensile test.

INTRODUCTION

Due to excellent processability, high chemical resistance, safety in contact with food products, desirable physical properties, and low cost, PE has received the most attention in different applications ranging from packaging industry to greenhouse covering, geomembrane and pipe applications [1-3]. However, some limitations such as poor rigidity and low gas barrier properties have restricted its application in some fields.

Research on polymer nanocomposites with very low clay content is an area of research that has seen a huge interest over the last two decades as a result of significant enhancement in properties such as stiffness and strength, flame retardancy, barrierity and thermal stability [4-9]. All these properties open up interesting prospects for use of these materials in a wide variety of applications [10-13].

Due to wide availability of the melt intercalation equipment, it is a common method in industrial prac-

* Corresponding Author - E-mail: abdorrasouli@hormozgan.ac.ir

tice for preparing thermoplastic nanocomposites. Some studies have shown that in this method the extent of clay intercalation is influenced by equipment type. The internal mixers and twin-screw extruders are the pieces of equipment commonly used for producing nanocomposites [14, 15].

A high intercalation level requires favorable polymer–clay interactions as well as optimum processing conditions. It is usually a difficult task to produce PE nanocomposites with a desirable structure, due to the very weak interactions between the polyethylene molecules and the polar surface of clays. Chungui Zhao et al. showed that the partially exfoliated structure formed in PE/nanoclay nanocomposites due to incorporation of modified montmorillonite clay was obtained due to the presence of a reactive intercalating agent, while only conventional microcomposites were obtained with adding the common alkylammonium intercalated clay [16]. Modified polymers having polar groups, also called compatibilizers, can be introduced into nanocomposite formulations to enhance the extent of intercalation [17, 18]. Pegoretti et al. showed that the presence of a PE-g-MA compatibilizer in PE/nanoclay samples increased the nanoclay interlayer d-spacing. They also demonstrated that the extent of melt intercalation increased as the PE matrix melt viscosity decreased (higher MFR) [19]. Durmus et al. explained that in PE/nanoclay nanocomposites a better dispersion was achieved with incorporation of a maleic anhydride grafted polyethylene (PE-g-MA) compatibilizer than that obtained with incorporation of an oxidized PE (OxPE) compatibilizer [20]. Sanchez-Valdes et al. showed that a more effective intercalation and dispersion condition could be obtained in the preparation of compatibilized PE/nanoclay nanocomposites performed by two-step twin-screw melt mixing compared to one-step melt mixing [21].

In polymer/nanoclay nanocomposites, the extent of intercalation and degree of dispersion of clay can be evaluated by X-ray diffraction (XRD) along with transmission electron microscopy (TEM). Although XRD offers a convenient method to determine the interlayer spacing in the original clay layers and intercalated structure, a little information can be obtained about the spatial distribution of clay layers and/or any disordered structure. In contrast to XRD, TEM provides very useful information about the dispersion state of clay particles in a wide range of length scales, but it is a time consuming and expensive technique

[22, 23].

It is well known that the rheological properties of multiphase systems including particulate suspensions are very sensitive to structure, size, shape, and surface characteristics of dispersed phase. Thus, the rheology can be employed as a powerful method in complementary to conventional methods such as XRD and TEM to study structure of polymer clay nanocomposites [24]. Moreover, the rheological studies provide valuable information about the processability of these materials in melt processing units such as extrusion and film casing process [25, 26].

Film is the largest market segment for polyethylene (PE). Improvements in properties of the PE films by incorporation of clay nanoparticles can promote current applications and even more advanced applications like horticultural product, electronic and pharmaceutical packaging. On the other, the ability of a polyethylene to be converted into film depends on its melt strength or equivalent rheological properties, like the elongational viscosity and viscoelastic behavior that can be affected by incorporation of clay.

Some literature shows the effect of film processing parameters such as draw down ratio and blow up ratio on mechanical and gas barrier properties of polyethylene/nanoclay nanocomposite blown films [8, 27–29]. However, there is no report on the effect of processing parameters on structure development and mechanical properties of PE/clay nanocomposite cast films.

The aim of this work was studying the effects of mixer type, clay content, feeding order and draw ratio on the structure development, rheological, thermal and mechanical properties of PE/nanoclay nanocomposites and PE/nanoclay nanocomposite cast films.

EXPERIMENTAL

Material

Two commercial film grades, a linear low density polyethylene (SW218) with melt flow index 2 g/10 min (190°C and 2.16 kg) and a low density polyethylene (HP2022) with melt flow index 2 g/10 min (190°C and 2.16 kg) supplied by SABIC were used as matrices.

A commercial maleic anhydride-grafted polyethylene (Orevak_18302n) with melt flow index 1.2 g/10min (190°C and 2.16 kg) was purchased from Arkema and used as compatibilizer.

A natural montmorillonite modified with a quaternary ammonium salt with a cation exchange capacity of 125 meq/100g clay Cloisite 15A (CL15A) from Southern Clay, Inc., was used as a nanofiller.

Melt blending

The polymer nanocomposite samples listed in Table 1 were considered. The weight ratio of compatibilizer/nanoclay for all nanocomposites was taken constant as 2. These samples were blended in a variety of mixers and feeding orders.

Nanocomposite samples were prepared in a Brabender internal mixer (GmbH & Co. W50 model, Germany) with a normal capacity of 60 mL and a roller type blade, and also in a Haake Rheomix 3000 batch internal mixer with a Haake System 90 drive (Thermo Fisher Scientific Inc., USA) having a normal capacity of 350 mL and a roller type blade operated at 160°C for 20 min with a rotor speed of 70 rpm. Other samples were prepared in a Brabender co-rotating twin-screw extruder DSE25 with a barrel diameter of 25 mm and L/D=40. The temperature of the extruder was maintained at 150, 160, 170, 180, 180, and 180°C from hopper to die, and the screw speed was fixed at 150 rpm. The average shear rates of different mixers were estimated using an empirical calibration technique developed by Marquez et al. [30] to be about 21, 26 and 48 s⁻¹ for the Haake Rheomix and Brabender W50 internal mixers and twin-screw extruder DSE25, respectively.

To study the effect of feeding order, two different feeding orders were used: (1) simultaneous feeding, and (2) LLDPE-g-MA compatibilizer/nanoclay masterbatch feeding. In the later feeding procedure, the

LLDPE-g-MA/nanoclay masterbatch was first prepared during 10 min and then mixed with LLDPE for 10 min as a matrix.

The LLDPE/nanoclay samples prepared in the Haake Rheomix lab internal mixer were converted into films by using a Brabender single-screw extruder (Plasticorder PL200) equipped with a slit die and a take-up roll device. Three different draw ratios (DRs) of 1, 10 and 20 were used to produce the films. The temperatures of three heating zones and die of the single-screw extruder were 180, 190, 190, and 190°C, and the screw speed was 30 rpm.

Characterization

XRD patterns of the samples were recorded on a Rigaku X-ray diffractometer with nickel-filtered Cu-K α radiation ($\lambda=0.154$) operated at 50 kV and 150 mA. Data were obtained over the range $2\theta = 1.5^\circ$ to 10° .

Rheological measurement of the samples were studied by using a rheometric mechanical spectrometer (Paar Physica USD200), with a parallel plate (diameter = 2.5 cm; gap = 1 mm) geometry at 175°C and at a strain of 1% to ensure the linear viscoelastic region. Linear melt state viscoelastic behavior of the samples was studied using frequency sweep experiment in small strain oscillatory shear deformations.

Nonisothermal crystallization behavior of the samples was determined using a SHIMADZU DSC-60 differential scanning calorimeter. In the nonisothermal crystallization process, the samples were first heated from room temperature to 160°C at a rate of 5°C/min, then held at 160°C for 5 min to eliminate the thermal history. Then, the samples were cooled to room temperature at a rate of 5°C/min. The heating and cooling

Table 1. samples recipes, mixing conditions and feeding orders.

Sample ^(a)	LLDPE (w.t. %)	LDPE (w.t. %)	Nanoclay (w.t. %)	Mixer type	Feeding order
LL2B	94	-	2	Brabender internal mixer	1
LL4BM	88	-	4	Brabender internal mixer	2
LL4B	88	-	4	Brabender internal mixer	1
LL4H	88	-	4	Haake internal mixer	1
LL4T	88	-	4	Brabender twin screw extruder	1
LL6B	82	-	6	Brabender internal mixer	1
LD4B	88	-	4	Brabender internal mixer	1
LL4B	88	-	4	Brabender internal mixer	1
LL4B	88	-	4	Brabender internal mixer	1
LD2B	-	94	2	Brabender internal mixer	1
LD4B	-	88	4	Brabender internal mixer	1
LD6B	-	82	6	Brabender internal mixer	1

^(a) The weight ratio of compatibilizer/nanoclay for all nanocomposites was taken constant as 2.

rates were 10°C/min. The basic equation for calculation of X_c of the hybrid using DSC data is as follows:

$$X_c = \frac{\Delta H}{(1-\phi)\Delta H_{100}} \quad (1)$$

where ϕ is the weight percent of nanoclay; ΔH is the integrated melting enthalpy; ΔH_{100} is the melting enthalpy of 100% crystalline polyethylene, which is taken as 287.3 J/g in this study [20].

Mechanical tests were carried out with using a Galdabini Sun 2500 tensile tester (Galdabini, Italy) according to ASTM D882.

RESULTS AND DISCUSSION

XRD and TEM results

XRD patterns of the nanoclay (Cloisite 15A) are given in Figure 1. As it can be seen, the nanoclay showed two characteristic diffraction peaks at $2\theta = 2.8^\circ$ and $2\theta = 7.3^\circ$. The peak observed at $2\theta = 2.8^\circ$ corresponded to the interlayer spacing of the modified layers of montmorillonite, while the peak observed at $2\theta = 7.3^\circ$ was related to the unmodified layers.

Figure 2 shows the XRD patterns of the LLDPE/nanoclay and LDPE/nanoclay samples, which have the same compatibilizer/nanoclay weight ratio, but different nanoclay contents. These results showed that the main characteristic peak of nanoclay in both series of nanocomposites shifted toward lower angle as a result of melt intercalation. It was worth mentioning that the extent of melt intercalation in the LDPE/nanoclay

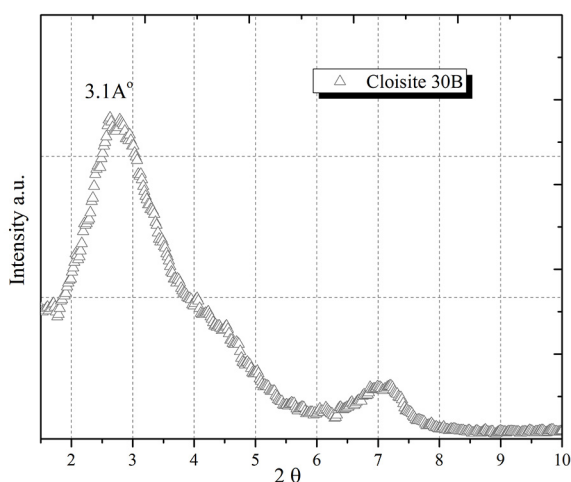


Figure 1. X-Ray diffraction patterns of the Cloisite 15A.

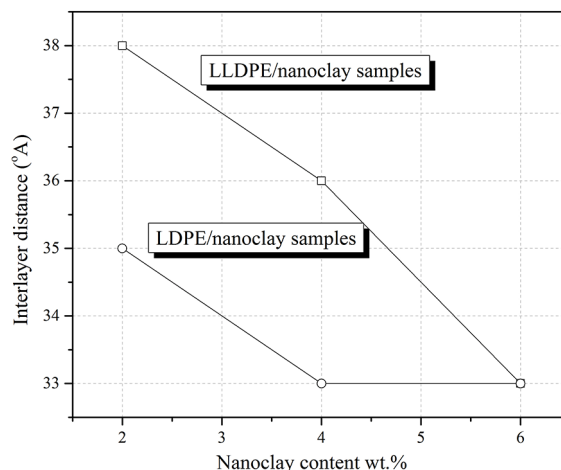


Figure 3. Interlayer d-spacing of the nanoclay corresponded to the main characteristic peak of both LLDPE/nanoclay and LDPE/nanoclay samples.

samples was lower than that in the LLDPE/nanoclay samples as results of hindrance effect of long chain branches in LDPE matrix and lower compatibility between LDPE and LL-g-MA compatibilizer.

Figure 3 shows the nanoclay interlayer d-spacing of the compatibilized LLDPE/nanoclay and LDPE/nanoclay samples as a function of nanoclay content. As it can be seen, although the samples have the same weight ratio of compatibilizer to nanoclay ($\alpha = 2$) and the melt viscosity of these samples increases with increase of nanoclay content (specially above 10 s^{-1} which was in the range of frequency estimated from the shear rate induced by internal mixer (see Figures 7 and 8)), the interlayer d-spacing of the nanoclay decreases. This suggested that the increase in the shear

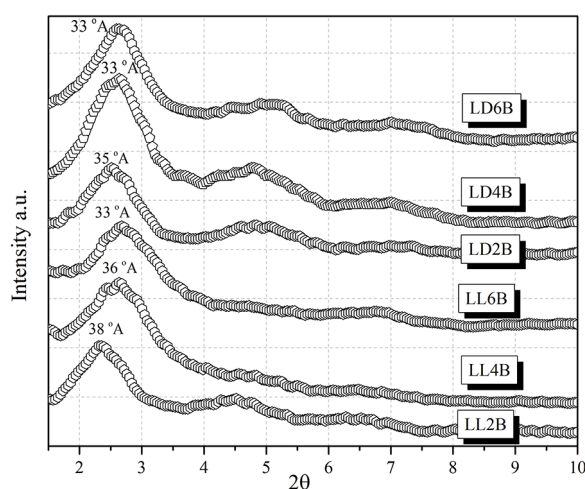


Figure 2. X-Ray diffraction results of the LLDPE/nanoclay and LDPE/nanoclay samples.

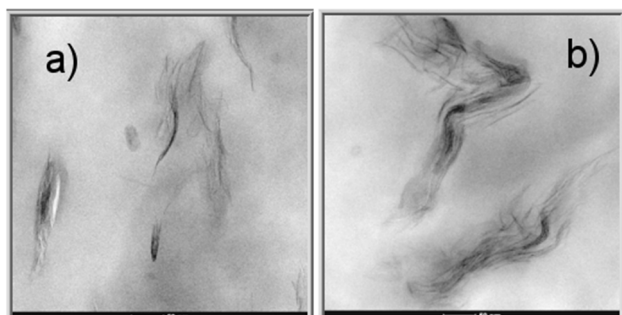


Figure 4 TEM images of LLDPE/nanoclay and LDPE/nanoclay nanocomposites both containing 4 wt.% nanoclay.

stress transferred to nanoclay due to increase in viscosity did not allow to increase nanoclay melt intercalation. It seemed to be necessary for a more compatibilizer content, which was more than twice as much as nanoclay content (for the systems analyzed in the present work), in order to maintain constant the capability of polyethylene chains to diffuse into the interlayer d-spacing of the nanoclay platelets.

To support the observed XRD results, the degree of dispersion and melt intercalation of nanoclay in the PE system were studied by TEM. TEM images of LLDPE-based and

LDPE-based nanocomposites both containing 4 wt.% nanoclay, shown in Figure 4, revealed the intercalated structure in which the PE chains were inserted into the interlayer spacing of the nanoclay platelets and/or tactoids. According to this result one may also notice that the better dispersion and melt intercalation of nanoclay observed in the LLDPE/nanoclay samples compared to those obtained in the LDPE/nanoclay samples are in agreement with the results obtained from the XRD tests.

In Figure 5 the XRD patterns of the LLDPE/nanoclay samples containing 4 wt.% cloisite 15A prepared by using the Brabender internal mixer (LL4B), Haake internal mixer (LL4H) and Brabender twin-screw extruder (LL4T) are compared. As it can be seen, the main characteristic peak of the LL4T sample shifts toward the lower angle in comparison with that of the LL4B and LL4H samples. This implies that the twin-screw extruder is more effective in melt intercalation of nanoclay in the LLDPE/nanoclay sample as a result of high shear stress generation.

Rheological results

Figure 6 shows the storage modulus and complex viscosity as a function of frequency for virgin LLDPE,

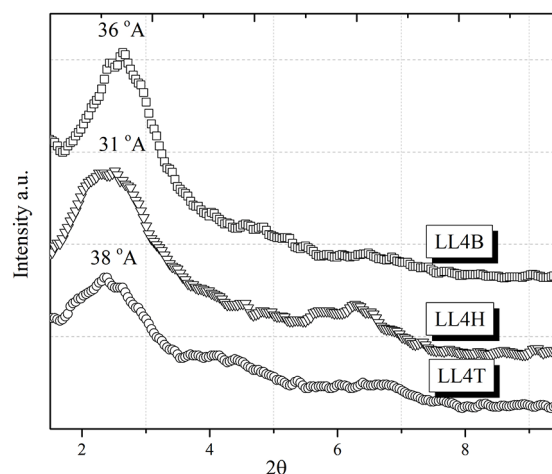


Figure 5 X-Ray diffraction results of the LLDPE/nanoclay samples containing 4 wt.% cloisite 15A prepared in the Brabender internal mixer (LL4B), Haake internal mixer (LL4H) and twin-screw extruder (LL4T).

LL4B, LL4BM, LL4H and LL4T samples. Table 2 shows the percentage increase in storage modulus values for these samples compared to that for virgin LLDPE (LL), at frequency 0.1 s^{-1} . As it can be seen, the melt elasticity and complex viscosity of the sample prepared by the twin-screw extruder are greater than those of samples prepared by both type of the internal mixers, at low frequency (the percentage increase in the storage modulus values of LL4T, LL4B and LL4H compared to that of virgin LLDPE at frequency 0.1 s^{-1} are 1500%, 1200% and 600%, respectively). This suggested that the dispersive ability of the mixers ranged in the following order: Brabender twin-screw extruder > Brabender internal mixer > Haake internal mixer in accordance with the XRD results. From

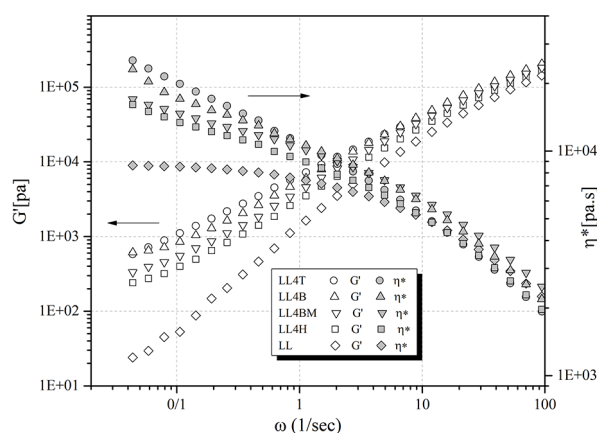


Figure 6 Storage modulus and complex viscosity vs. frequency for virgin LLDPE, LL4B, LL4BM, LL4H and LL4T samples.

these results, it could also be observed that the sample prepared by masterbatch (LL4BM) and simultaneous feeding (LL4B) exhibited 700% and 1200% percentage increase in storage modulus value at frequency 0.1 s^{-1} , respectively. The greater melt elasticity and pronounced non-terminal behavior of simultaneous feeding (LL4B) can be considered as indication of stronger three-dimensional (3D) networks structure formed in the this sample as a result of greater extent of intercalation and better dispersion of nanoclay in PE matrix as compared to that of masterbatch feeding sample (LL4BM).

Figures 7 and 8 show the storage modulus and complex viscosity of LLDPE and LDPE based nanocomposites as a function of frequency, respectively, with different nanoclay loadings. Table 2 also shows the percentage increase in the storage modulus values for these samples compared to the virgin PE (LLDPE and LDPE), at frequency 0.1 s^{-1} . It is clearly seen that the nanoclay influences the storage modulus, especially at low frequencies. For both series of the nanocomposites, as the nanoclay amount increases, magnitude of

Table 2. Storage Modulus Values and Percentage Increase in Storage Modulus Values for Some Samples, at Frequency 0.1 s^{-1} .

Sample	G' [pa]	Percentage change in G'
Virgin LLDPE	53	-
LL4T	741	$\frac{G'_{LL4T} - G'_{LL}}{G'_{LL}} \approx 1500$
LL4B	724	$\frac{G'_{LL4B} - G'_{LL}}{G'_{LL}} \approx 1200$
LL4H	318	$\frac{G'_{LL4H} - G'_{LL}}{G'_{LL}} \approx 600$
LL2B	179	$\frac{G'_{LL2B} - G'_{LL}}{G'_{LL}} \approx 200$
LL4B	724	$\frac{G'_{LL4B} - G'_{LL}}{G'_{LL}} \approx 1200$
LL6B	1900	$\frac{G'_{LL6B} - G'_{LL}}{G'_{LL}} \approx 3400$
Virgin LD	621	-
LD2B	973	$\frac{G'_{LD2B} - G'_{LD}}{G'_{LD}} \approx 60$
LD4B	1900	$\frac{G'_{LD4B} - G'_{LD}}{G'_{LD}} \approx 200$
LD6B	3390	$\frac{G'_{LD6B} - G'_{LD}}{G'_{LD}} \approx 450$

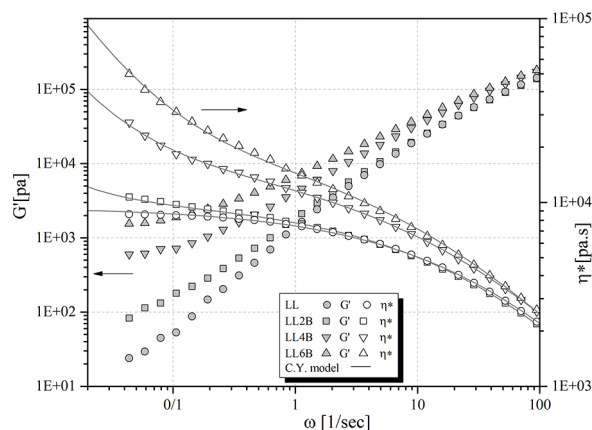


Figure 7. Storage modulus and complex viscosity of LLDPE/nanoclay nanocomposites as a function of frequency (comparison of experimental data with C.Y model).

the storage modulus increases and slope of the storage modulus decreases at low frequency region, resulted from increasing tactoids concentration and, therefore, greater extent of structure formation.

From these Figures, it can also be seen that there is no apparent yield stress for virgin polyethylene (LLDPE and LDPE), nevertheless, the nanocomposites show a viscosity upturn at low frequencies. A Carreau–Yasuda model with yield stress can be used to describe such material behavior as follows [31]:

$$\eta^* = \frac{\sigma_0}{\omega} + \eta_0 \left[1 + (\lambda\omega)^a \right]^{(m-1)/a} \quad (2)$$

where σ_0 is the melt yield stress, η_0 is the Newtonian viscosity, λ is a characteristic relaxation time, m is the shear thinning index, and a is the Yasuda parameter.

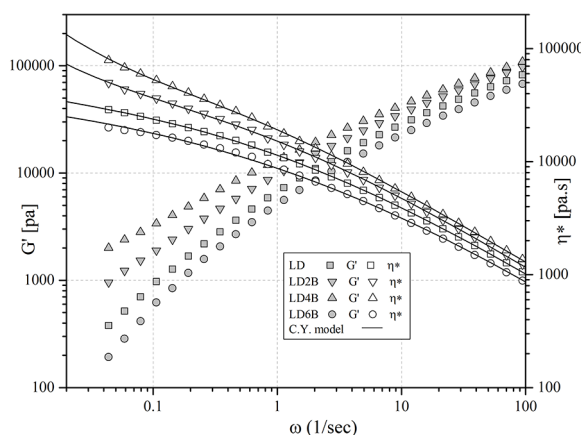


Figure 8. Storage modulus and complex viscosity of LDPE/nanoclay nanocomposites as a function of frequency (comparison of experimental data with C.Y model).

Solid lines in **Figures 7** and **8** represent the best fits of experimental data using Eq. (1), confirming the relevance of the chosen model. The complex viscosity in the low frequency regime can be described using either σ_0 or the plateau value of the storage G'_p and loss G''_p moduli.

$$\eta^* = \frac{\sigma_0}{\omega} \quad \text{for } \omega < 1 \quad (3)$$

$$\eta^* = \frac{1}{\omega} \sqrt{(G'_p)^2 + (G''_p)^2} = \frac{G_p^*}{\omega} \quad \text{for } \omega < 1 \quad (4)$$

where G_p^* is the complex modulus plateau at low frequency. Combining Eq. (3) with Eq. (4), we can write:

$$\sigma = G_p^* \quad (5)$$

Moreover, since elasticity was dominant in these systems, $|G_p^*|$ (and thus σ_0) was close to G'_p . However, as storage modulus plateau was often not perfectly developed at low nanoclay contents for the investigated angular frequency range, the melt yield stress was preferred. The scaling behavior of the elastic properties for fractal networks, developed by Shih et al. can be used to quantitatively analyze the rheological data. Shih et al. [32] deliberated that the structure of a particle network is a collection of fractal aggregates linked elastically together. In this case, low frequency solid body response was dominated by the elasticity of the backbones of the aggregates (the link between particles in an aggregate network was approximated by the spring. The backbone of aggregates was similar to a linear chain of springs formed from rows of particles in which 3D-structures were attached). In this regime, the value of the plateau modulus was predicted to have a power law dependence on volume fraction:

$$G'_p = \sigma_0 \propto \phi^{(3+x)/(3-d_f)} \quad (6)$$

where x referred to the chemical length and d_f is the fractal dimension. Potanin [33] considered d_f/x as an invariant and proposed $d_f/x = 3/2$ for three-dimensional networks.

Figure 9 shows the values of melt yield stress (σ_0) of the LLDPE and LDPE nanocomposite series against nanoclay volume fraction. By applying fractal scaling concept for our samples, the melt yield stresses of the LLDPE and LDPE nanocomposite series scale as $\phi^{3.1}$ corresponded to $d_f = 1.67$ and $\phi^{3.57}$ corresponded

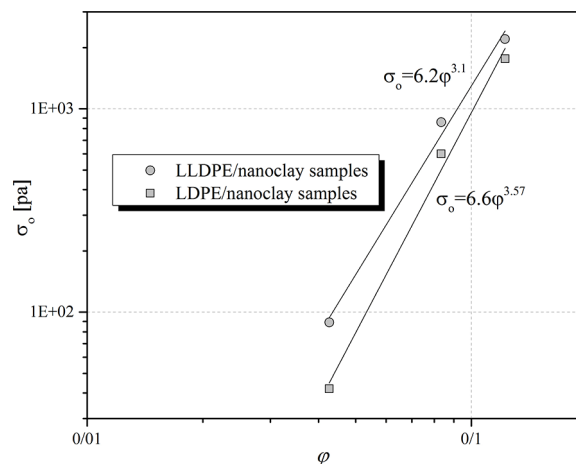


Figure 9. Values of melt yield stress (σ_0) of LLDPE/nanoclay and LDPE/nanoclay nanocomposite series against clay volume fraction.

to $d_f = 1.81$, respectively. One may also notice that the higher value of fractal dimension for the LDPE nanocomposites can be explained by the worst nanoclay dispersion with a less open fractal structure (more dense structure) due to the hindrance effect of the long chain branches of LDPE matrix and lower compatibility between LDPE and LL-g-MA compatibilizer as compared to LLDPE nanocomposites.

DSC results

The nonisothermal crystallization thermograms of the virgin LLDPE (LL), polyethylene containing 8 wt.% LL-g-MA compatibilizer and compatibilized LLDPE nanocomposite containing 4 wt.% nanoclay (LL4H) obtained from the cooling scan are shown in **Figure**

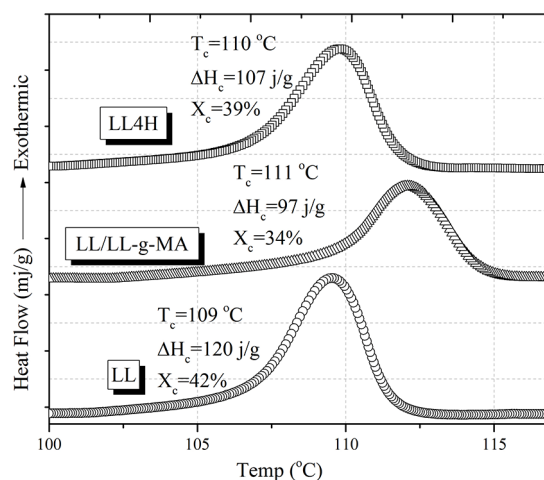


Figure 10. DSC curves of virgin LLDPE, the polyethylene sample containing 8 wt.% compatibilizer and compatibilized LLDPE/nanoclay nanocomposite (LL4H).

10. The calorimetric parameters of the samples derived from DSC analysis are also shown in this figure. T_c is the crystallization temperature peak, and ΔH_c is the enthalpy of crystallization normalized to unit mass of LLDPE matrix. $X_c\%$, the degree of crystallinity of the samples, was calculated by comparing ΔH_c with that for an infinitely large crystal of LLDPE (287.3 J/g) [34]. As it can be seen, the incorporation of 4 wt.% nanoclay into LL/LL-g-MA decreases T_c by about 1.5°C and increases $X_c\%$ by about 5%. It was suggested that there existed two competing aspects during the crystallization process of the nanocomposites. First, the nanoclay can provide a heterogeneous surface and facilitate the nucleating rate of macromolecules; second, the interfacial interactions between the surface of nanoclay and polar maleic anhydride groups of grafted chains can hinder the motions of molecules, leading to decrease in the growing rate. It seemed that the latter aspect became dominate in the LL4H samples which could lead to the decrease of T_c and the formation of crystallites with more defects and, therefore, the decrease of the crystallinity. It can be also seen that the addition of compatibilizer (LL-g-MA) to the LLDPE increases T_c by about 2.5°C and decreases X_c by about 10%. These may be explained by the nucleation effect of LL-g-MA similar to that of LLDPE/EVA blend [35], leading to the formation of lamellar crystals with more defects and, therefore, decreasing the crystallinity.

Characterization of cast films

Nanoclay intercalation was analyzed by XRD for the

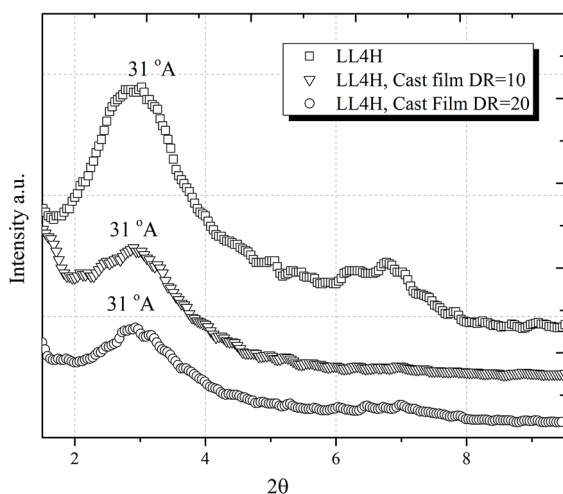


Figure 11. X-Ray diffraction results of LLDPE/nanoclay cast films and LL4H sample (before formation of film).

LLDPE/nanoclay cast films and the sample LL4H (before formation of film), as shown in Figure 11. As it can be seen, the sample LL4H shows two characteristic peaks at $2\theta = 2.8^\circ$ and $2\theta = 6.8^\circ$, and both the cast films exhibit one broad distinguished characteristic peak at $2\theta \approx 2.8^\circ$, whose intensity is less than that of LL4H. This suggested that the film-casting process led to increase in melt intercalation of nanoclay.

Figure 12 shows the data of storage modulus and complex viscosity measured as a function of frequency for the LLDPE/nanoclay cast films containing 4 wt.% nanoclay. As it can be seen, with increasing the draw ratio, the non-terminal storage modulus and viscosity upturn are more pronounced. These may be attributed to strengthening of 3D network structure formed between nanoclay platelets as a result of increasing in melt intercalation due to the extensional flow field produced by cast film process in according to the XRD results.

The non-terminal behavior of the filled samples can be described by fractional generalization of the Zener model which contains of two fractional elements in series connected with a spring in a parallel manner [36, 37]. The constitutive equation of the model is given by the following equations:

$$\sigma + \tau_0^\alpha \frac{d^\alpha \sigma}{dt^\alpha} = G_e \left(\gamma + \tau_0^\alpha \frac{d^\alpha \gamma}{dt^\alpha} \right) + G_0 \tau_0^\beta \frac{d^\beta \gamma}{dt^\beta} \quad (7)$$

$$\alpha = \beta_1 - \beta_2 > 0 \text{ and } \beta = \beta_1$$

Here β_1 , τ_0 , G_0 and G_e represent the fractional exponents, characteristic time, modulus of fractional ele-

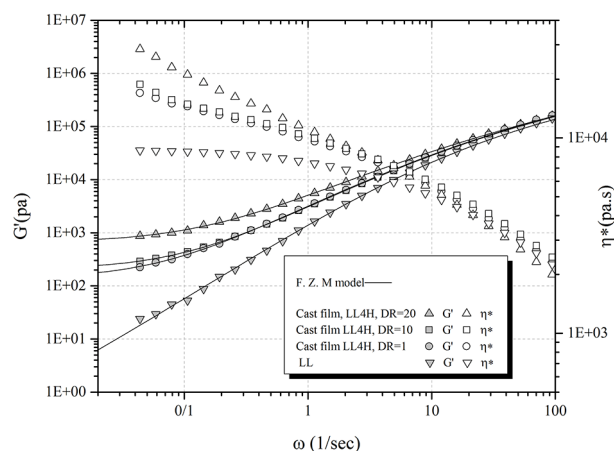


Figure 12. Storage modulus and complex viscosity as a function of frequency for the LLDPE/nanoclay cast films. Comparison of experimental and theoretical results (F. Z. M. data).

ments and elastic modulus of the spring, respectively. Rheological behavior of the fractional elements changes range from purely viscous when $\beta=1$ to purely linear elastic when $\beta=0$. According to the constitutive equation of this model, the complex modulus and, therefore, the storage and loss modulus are described by the following equations [38]:

$$G^*(\omega) = G_e + G_0 \frac{(i\omega\tau_0)^\beta}{1 + (i\omega\tau_0)^\alpha} \quad (8)$$

$$G'(y) = G_e + G_0 y^\beta \frac{\cos(\beta\pi/2) + y^\alpha [(\beta - \alpha)\pi/2]}{1 + 2y^\alpha \cos(\alpha\pi/2) + y^{2\alpha}} \quad (9)$$

$$G''(y) = G_0 y^\beta \frac{\cos(\beta\pi/2) + y^\alpha [(\beta - \alpha)\pi/2]}{1 + 2y^\alpha \cos(\alpha\pi/2) + y^{2\alpha}} \quad (10)$$

$$y = \omega\tau_0$$

Table 3 shows the five parameter of eq (8) used to fit experimental data obtained for filled cast films with FZM model by taking into account the condition $\beta \leq 1$. The good agreement between the model and the data demonstrates the applicability of the model (see Figure 12). The low-frequency behavior of the virgin LLDPE was described by the fractional exponent $\beta_1=1$ and a zero elastic modulus G_e . As it can be seen, for the filled cast films, β_1 parameter decreased and G_e parameter increased with increase in the draw ratio as a result of network structure strengthening, as discussed earlier.

The machine direction modulus (E), yield strength (YS) and elongation-at-break (EB) of the virgin LLDPE cast films and LLDPE nanocomposite cast films containing 4 wt.% nanoclay (LL4H cast films) as a function of draw ratio are shown in Figures 13, 14 and 15, respectively. These results show that both machine direction modulus and yield strength of the LL4H cast films decrease significantly with increase of draw ratio from 1 to 10, and the rate of reduction of these properties decreases with increase of draw ratio from 10 to 20. A similar trend was observed for virgin LLDPE

Table 3. Fit parameters of the FZM.

Sample	β_1	α	τ_0	G_e	G_0
LL	1	0.54	0.09	0	100000
Cast film LL4H, DR=1	0.94	.49	0.11	202	100000
Cast film LL4H, DR=10	0.92	0.48	0.1	290	100000
Cast film LL4H, DR=20	0.88	0.45	0.12	648	100000.4

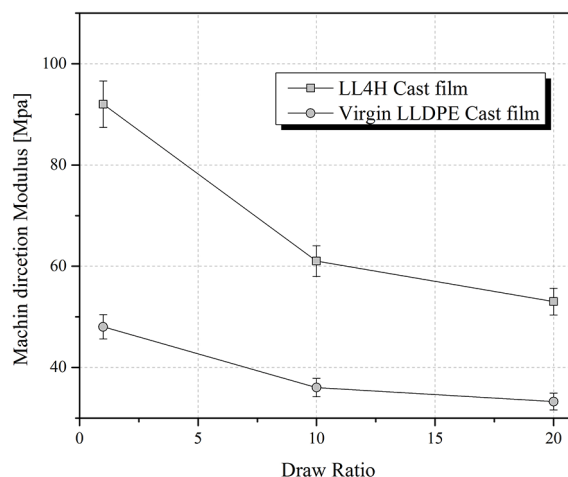


Figure 13. Machine direction modulus (E) of virgin LLDPE cast films and LLDPE/nanoclay nanocomposite cast films as a function of draw ratio.

cast films. This could be explained in terms of reducing degree of crystallinity, orientation of PE matrix (or nanoclay tactoids) and intercalation of nanoclay as competitive parameters. Increase of draw ratio resulted in more effective cooling rate process due to increasing heat transfer area of the films which could lead to reducing degree of crystallinity and, therefore, decreasing both machine direction modulus and yield strength. In other hand, both the rheological and XRD results showed that the increase of draw ratio resulted in the increase of melt intercalation and better dispersion of nanoclay (especially at the higher draw ratio, as discussed earlier) and, therefore, increasing the reinforcement effect of nanoclay. Also it can be

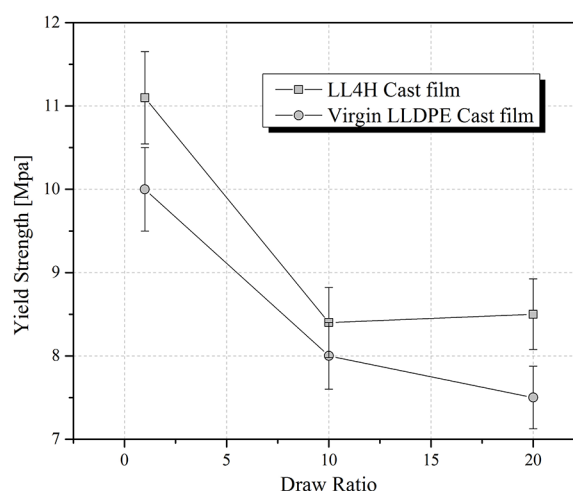


Figure 14. Yield strength (YS) of virgin LLDPE cast films and LLDPE/nanoclay nanocomposite cast films as a function of draw ratio.

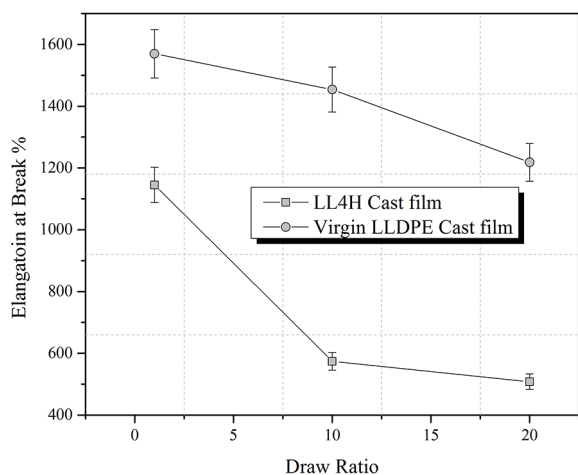


Figure 15. Elongation-at-break (EB) of virgin LLDPE cast films and LLDPE/nanoclay nanocomposite cast films as a function of draw ratio.

expected that the increase of draw ratio can result in increase of macromolecular chains orientation and/or nanoclay tactoids in the machine direction, leading to increase of mechanical properties. In determination of the machine direction modulus and yield strength of the PE nanocomposite cast films, it seems that the degree of crystallinity reduction is the dominant parameter among the described competitive parameters.

According to these figures, it can also be noticed that the incorporation of 4 wt.% nanoclay into the cast films results in increasing of machine direction modulus and yield strength in whole of the draw ratio range, as compared to virgin LLDPE owing to the reinforcement effect of nanoclay. As regards the elongation-at-break (EB), the addition of nanoclay causes a decrease in this property with respect to the unfilled films, in whole of the draw ratio range, as seen in [Figure 15](#). This can be attributed to the stiffness induced in the filled samples by the formation of a network between the nanoclay and the polymer phase. As it can be observed in this figure, the elongation-at-break of both the filled and unfilled films decrease with increase of draw ratio as a consequence of orientation of PE matrix.

CONCLUSION

Three types of mixing machines including a Brabender twin-screw extruder, a Haake internal mixer (with a 350 mL capacity) and a Brabender internal mixer (with a 60 mL capacity) were used to prepare LLDPE/

nanoclay samples contacting 4 wt.% cloisite. It was shown that the sample prepared by the twin-screw mixer exhibited a pronounced low frequency non-terminal storage modulus and viscosity upturn, whose values were found to be greater than those of sample prepared by the internal mixers. This could be attributed to the greater potential of the twin-screw extruder in melt intercalation of nanoclay existed in comparison with the internal mixers. From the melt linear viscoelastic results obtained for the samples prepared by the simultaneous feeding and the compatibilizer/nanoclay masterbatch feeding, it was observed that the dispersion and intercalation of nanoclay in the sample prepared by masterbatch feeding was worse due to the trapping of more nanoclay particles in the compatibilizer and formation of a weaker 3D-network structure. Fractal scaling model showed that a better dispersion of nanoclay particles was achieved in the LLDPE than that in the LDPE in accordance with the XRD and TEM results. The results of linear melt viscoelastic measurement performed on the LLDPE/nanoclay cast films showed an increase of low frequency storage modulus with increasing draw ratio as a result of better melt intercalation. It showed that the hindered motions of molecules led to decrease in the growing rate of nucleates in the LLDPE/LL-g-MA/nanoclay sample containing 4wt% nanoclay, resulting in decrease of T_c . The tensile test showed that the incorporation of nanoclay into the cast films increased the machine direction modulus and yield strength, nevertheless, decreased the elongation-at-break. Moreover, in both the filled and unfilled cast films, the increase of draw ratio decreased their mechanical properties.

REFERENCES

1. Mourad AHI, Dehbi A (2014) On use of trilayer low density polyethylene greenhouse cover as substitute for monolayer cover. *Past Rubber Compos* 43 : 111-121
2. Ewais AMR and Rowe RK (2014) Effects of blown film process on initial properties of HPDE geomembranes of different thicknesses. *Geosynth Int* 21: 62-82
3. Weltschew M (2011) Comparison between material parameters of polyethylene grades and the test performance behaviour of packaging for the transport of dangerous goods. *Packag Technol Sci*

- 24: 361-371
4. Tian Y, Yu H, Wu S, Ji G, Shen J (2004) Study on the structure and properties of EVA/clay nanocomposites. *J Mater Sci* 39: 4301-4303
 5. Srinath G and Gnanamoorthy R (2007) Effect of organoclay addition on the two-body abrasive wear characteristics of polyamide 6 nanocomposites. *J Mater Sci* 42: 8326-8333
 6. Sheng D, Tan J, Liu X, Wang P, Yang Y (2011) Effect of organoclay with various organic modifiers on the morphological, mechanical, and gas barrier properties of thermoplastic polyurethane/organoclay nanocomposites. *J Mater Sci*. 46: 6508-6517
 7. Abdolrasouli MH, Nazockdast H, Sadeghi GMM, Babaei A (2014) Polylactide/polyethylene/organoclay blend nanocomposites: Structure, mechanical and thermal properties. *Polym Plast Technol Eng* 53: 1417-1424
 8. Arunvisut S, Phummanee S, Somwangthanaroj A, Effect of clay on mechanical and gas barrier properties of blown film LDPE/clay nanocomposites. *J Appl Polym Sci* 106: 2210-2217
 9. Al-Qadhi M, Merah N, Gasem ZM (2013) Mechanical properties and water uptake of epoxy/clay nanocomposites containing different clay loadings. *J Mater Sci* 48: 3798-3804
 10. Nigmatullin R, Gao F, Konovalova V (2008) Polymer-layered silicate nanocomposites in the design of antimicrobial materials. *J Mater Sci* 43: 5728-5733
 11. Hong SI, Rhim JW (2012) Preparation and properties of melt-intercalated linear low density polyethylene/clay nanocomposite films prepared by blow extrusion. *LWT - Food Sci Technol* 48: 43-51
 12. Gul S, Kausar A, Muhammad B, Jabeen S (2016) Research progress on properties and applications of polymer/clay nanocomposite. *Polym Plast Technol Eng* 55: 684-703
 13. Tang Y, Gao P, Ye L, Zhao C (2010) Organoclay-modified thermotropic liquid crystalline polymers as viscosity reduction agents for high molecular mass polyethylene. *J Mater Sci* 45: 5353-5363
 14. Dennis HR, Hunter DL, Chang D, Kim S, White JL, Cho, JW, Paul DR (2001) Effect of melt processing conditions on the extent of exfoliation in organoclay-based nanocomposites. *Polymer* 42: 9513-9522
 15. Ujianto O, Jollands M, Kao N (2015) Polyethylene/clay nanocomposites prepared in an internal mixer: Effect of processing variable on mechanical properties. *Adv Mat Res* 1105: 46-50
 16. Zhao C, Qin H, Gong F, Feng M, Zhang S, Yang M (2005) Mechanical, thermal and flammability properties of polyethylene/clay nanocomposites. *Polym Degrad Stab* 87: 183-189
 17. Santos KS, Liberman MAS, Oviedo RS, Mauler RS (2014) Polyolefin-based nanocomposites: The effect of organosilane on organoclay dispersion. *J Mater Sci* 49: 70-78
 18. Abdolrasouli MH, Behzadfae E, Nazockdast H, Sharif F (2012) Structure development and melt viscoelastic properties of PE/organoclay nanocomposite blown films. *J Appl Polym Sci* 125 (SUPPL. 1): E435-E444
 19. Pegoretti A, Dorigato A, Penati A (2007) Tensile mechanical response of polyethylene - clay nanocomposites. *Express Polym Lett* 1: 123-131
 20. Durmus A, Kasgoz A, Macosko CW (2007) Linear low density polyethylene (LLDPE)/clay nanocomposites. Part I: Structural characterization and quantifying clay dispersion by melt rheology. *Polymer* 48: 4492-4502
 21. Sánchez-Valdes S, López-Quintanilla M L, Ramírez-Vargas E, Medellín-Rodríguez FJ, Gutierrez-Rodríguez JM (2006) Effect of ionomeric compatibilizer on clay dispersion in polyethylene/clay nanocomposites. *Macromol Mater Eng* 291: 128-136
 22. Jeong HM, Kim BC, Kim EH (2005) Structure and properties of EVOH/organoclay nanocomposites. *J Mater Sci* 40: 3783-3787
 23. Abdolrasouli MH, Nazockdast H, Sadeghi GMM, Kaschta J (2015) Morphology development, melt linear viscoelastic properties and crystallinity of polylactide/polyethylene/organoclay blend nanocomposites. *J Appl Polym Sci* 132: DOI 10.1002/app.41300
 24. Dorigato A, Pegoretti A, Penati A (2010) Linear low-density polyethylene/silica micro- and nanocomposites: Dynamic rheological measurements and modelling. *Express Polym Lett* 4: 115-129
 25. Nazockdast E, Nazockdast H, Goharpey F (2008) Linear and nonlinear melt-state viscoelastic properties of polypropylene/organoclay nanocomposites. *Polym Eng Sci* 48: 1240-1249
 26. Tang Y, Gao P, Ye L, Zhao C, Lin W (2010) Or-

- ganoclay/thermotropic liquid crystalline polymer nanocomposites. Part V: morphological and rheological studies. *J Mater Sci* 45: 2874-2883
27. Golebiewski J, Rozanski A, Dzwonkowski J, Galeski A (2008) Low density polyethylene–montmorillonite nanocomposites for film blowing. *Eur Polym J* 44: 270-286
28. Lotti C, Isaac CS, Branciforti MC, Alves RMV, Liberman S, Bretas RES (2008) Rheological, mechanical and transport properties of blown films of high density polyethylene nanocomposites. *Eur Polym J* 44: 1346-1357
29. Shah RK, Krishnaswamy RK, Takahashi S, Paul DR (2006) Blown films of nanocomposites prepared from low density polyethylene and a sodium ionomer of poly(ethylene-co-methacrylic acid). *Polymer* 47: 6187-6201
30. Marquez A, Quijano J, Gaulin M (1996) A calibration technique to evaluate the power-law parameters of polymer melts using a torque-rheometer. *Polym Eng Sci* 36: 2556-2563
31. Carreau PJ, De KD, Chhabra RP (1997) *Rheology of polymeric systems: Principles and applications*. Hanser Publishers
32. Shih W-H, Shih WY, Kim S-I, Liu J, Aksay IA (1990) Scaling behavior of the elastic properties of colloidal gels. *Phys Rev A* 42: 4772-4779
33. Potanin AA (1991) On the mechanism of aggregation in the shear flow of suspensions. *J Colloid Interface Sci* 145(1): 140-157
34. Xie Y, Yu D, Kong J, Fan X, Qiao W (2006) Study on morphology, crystallization behaviors of highly filled maleated polyethylene-layered silicate nanocomposites. *J Appl Polym Sci* 100: 4004-4011
35. Li C, Kong Q, Zhao J, Zhao D, Fan Q, Xia Y (2004) Crystallization of partially miscible linear low-density polyethylene/poly(ethylene-co-vinylacetate) blends. *Mater Lett* 58: 3613-3617
36. Heymans N, Bauwens JC (1994) Fractal rheological models and fractional differential equations for viscoelastic behavior. *Rheo Acta* 33: 210-219
37. Friedrich C (1993) Mechanical stress relaxation in polymers: Fractional integral model versus fractional differential model. *J NonNewton Fluid* 46: 307-314
38. Sailer C, Handge UA (2007) Melt viscosity, elasticity, and morphology of reactively compatibilized polyamide 6/styrene acrylonitrile blends in shear and elongation. *Macromolecules* 40: 2019-2028